Supplement of Atmos. Chem. Phys., 21, 6297–6314, 2021
https://doi.org/10.5194/acp-21-6297-2021-supplement

Atmospheric Chemistry and Physics
Open Access
EGU

Supplement of

In-depth characterization of submicron particulate matter inter-annual variations at a street canyon site in northern Europe

Luis M. F. Barreira et al.

Correspondence to: Luis M. F. Barreira (luis.barreira@fmi.fi) and Hilkka Timonen (hilkka.timonen@fmi.fi)

S1 Supplemental graphics and results

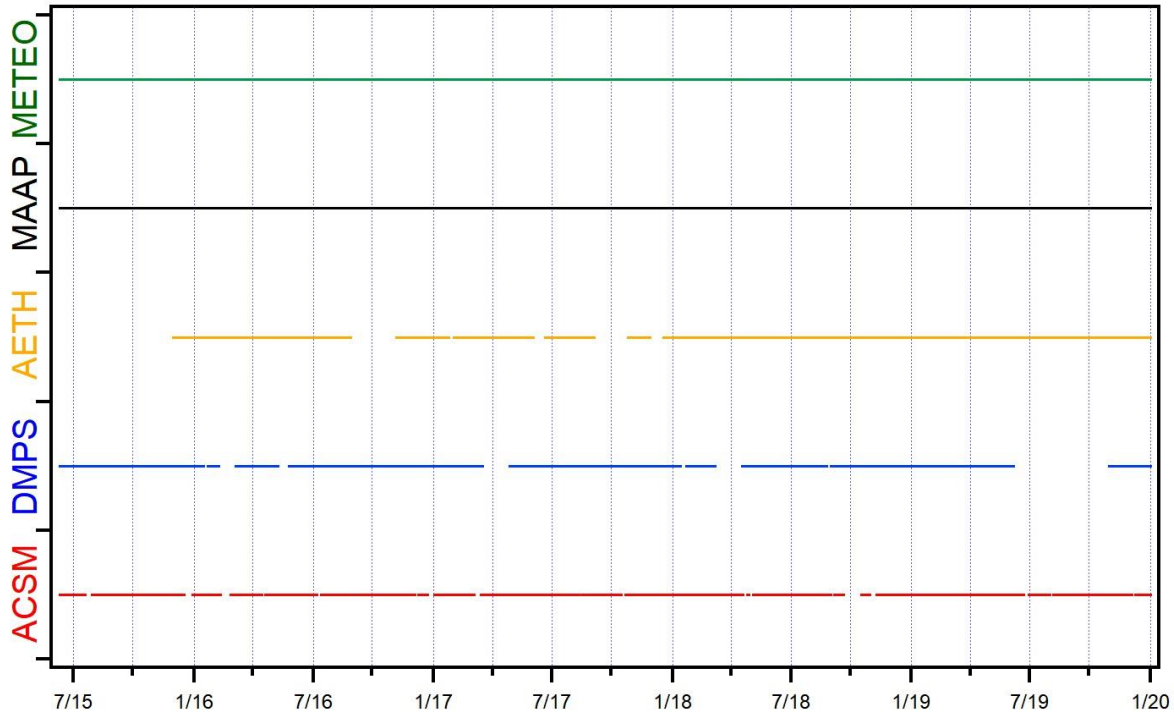

Figure S1: Measurement periods of instruments employed in this study.

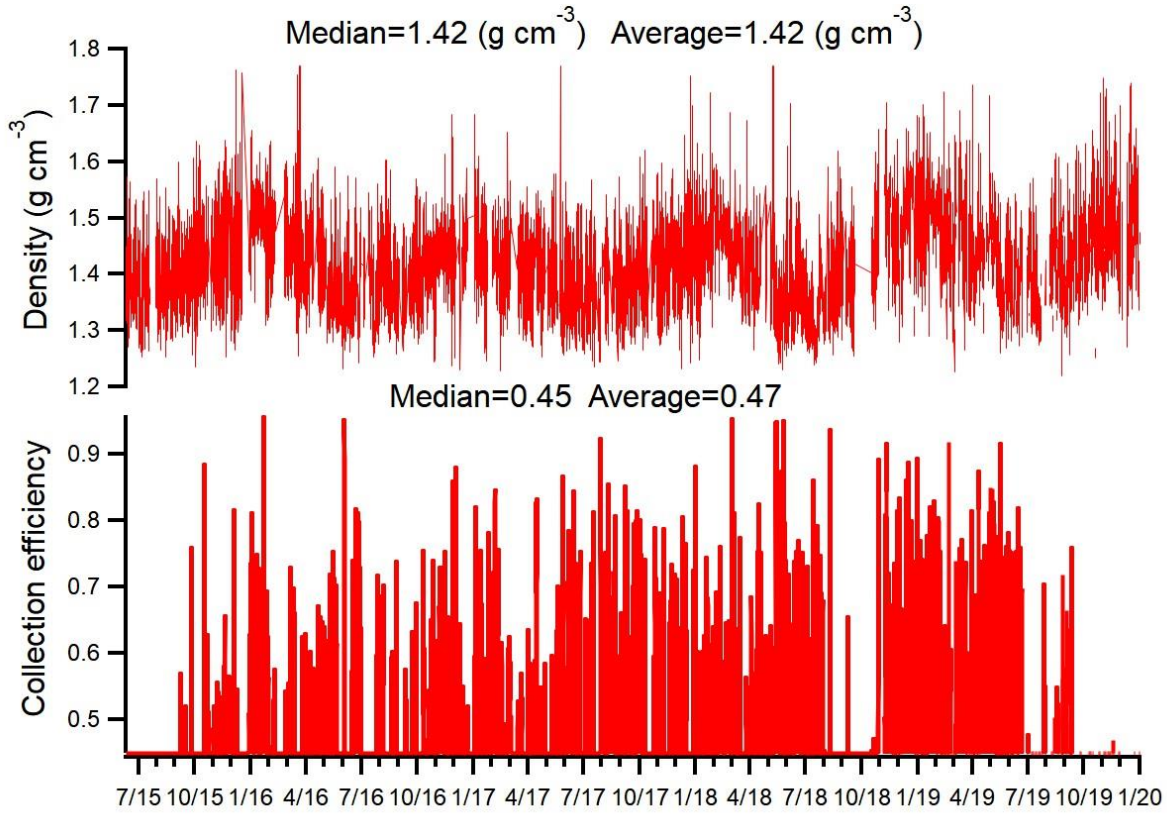

Figure S2: Density (top plot) and collection efficiency (bottom plot) determined during this study. Median and average values were included in the graphic.

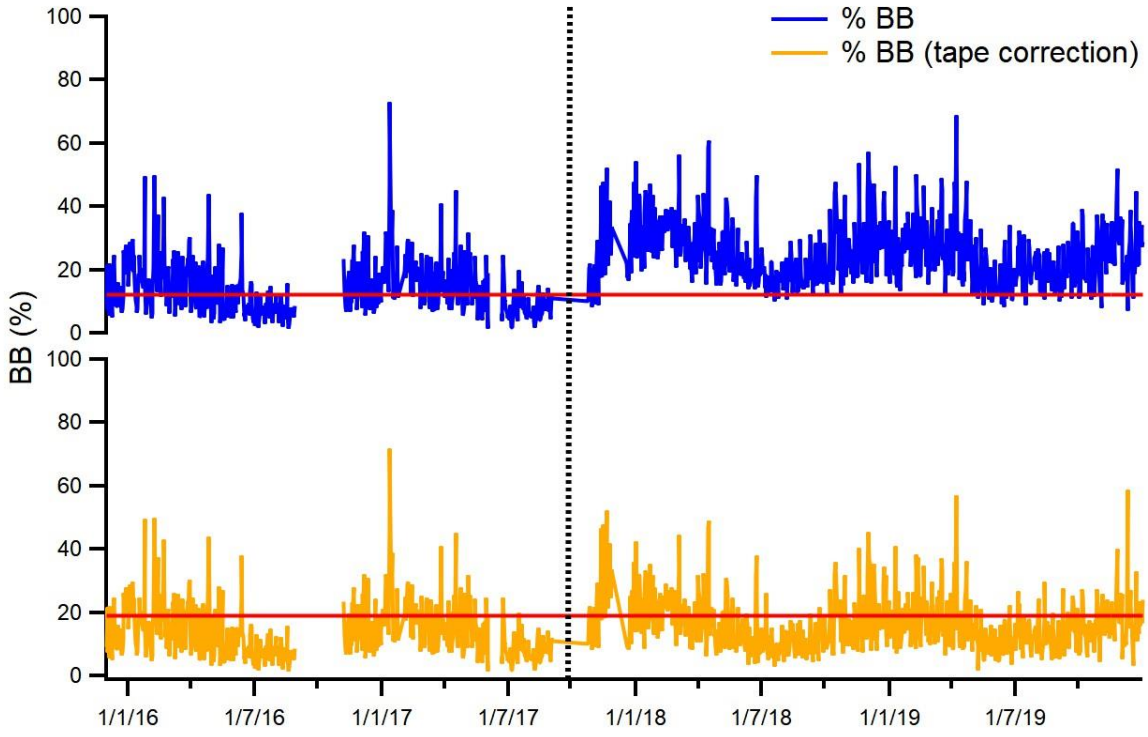

Figure S3: Correction applied to biomass burning (BB) percentage due to a change in the type of filter tape used during measurements. The red lines are the mean BB before correction (top plot) and during the entire period (bottom plot), while black line indicates the period after which the correction was applied.

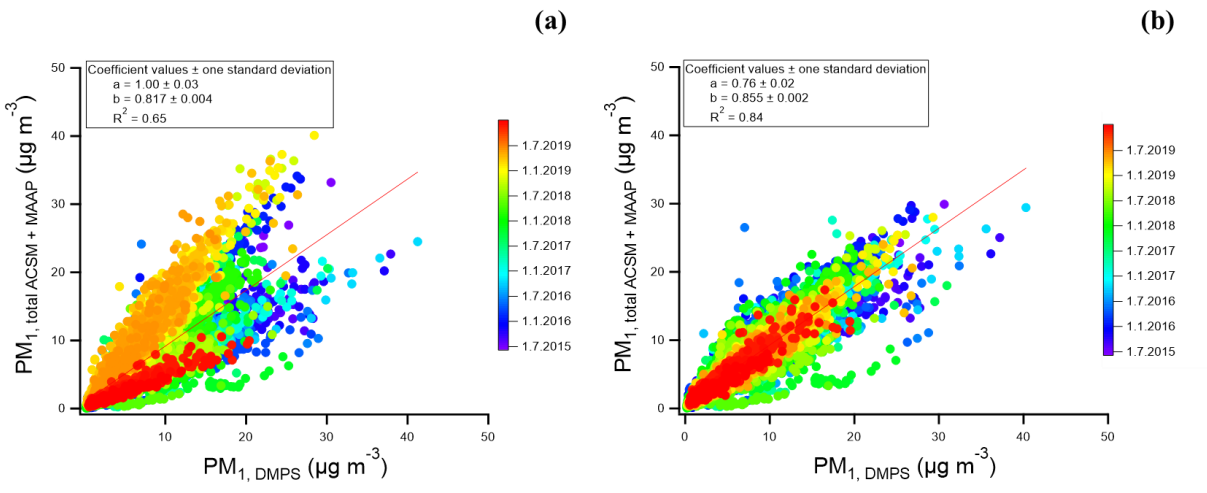

Figure S4: Total ACSM concentrations plus eBC measured by MAAP vs. PM_1 measured by DMPS, coloured according to the sampling time, before (a) and after (b) the employed correction. Slope coefficients and corresponding standard deviations were included.

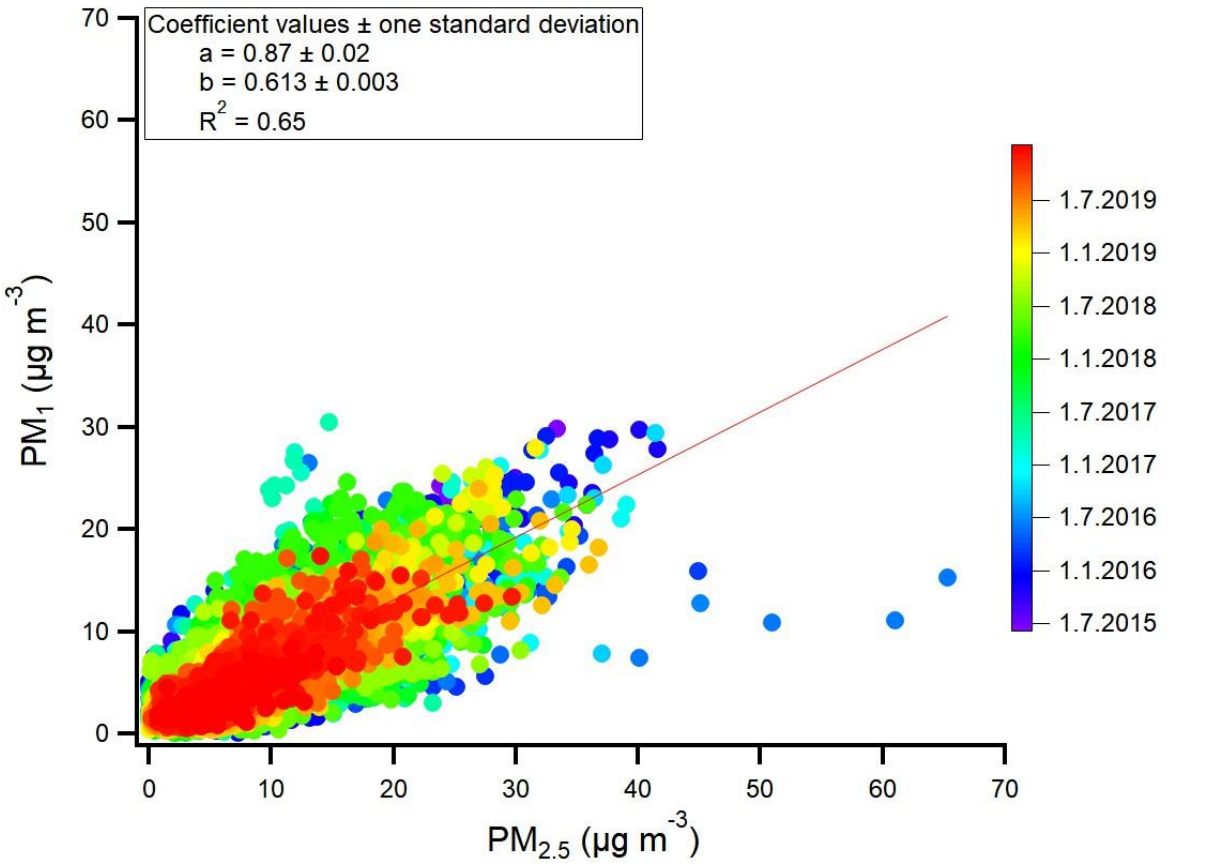

Figure S5: Total ACSM concentrations plus eBC measured by MAAP vs. $PM_{2.5}$ measured by TEOM, coloured according to the sampling time. Slope coefficients and corresponding standard deviations were included.

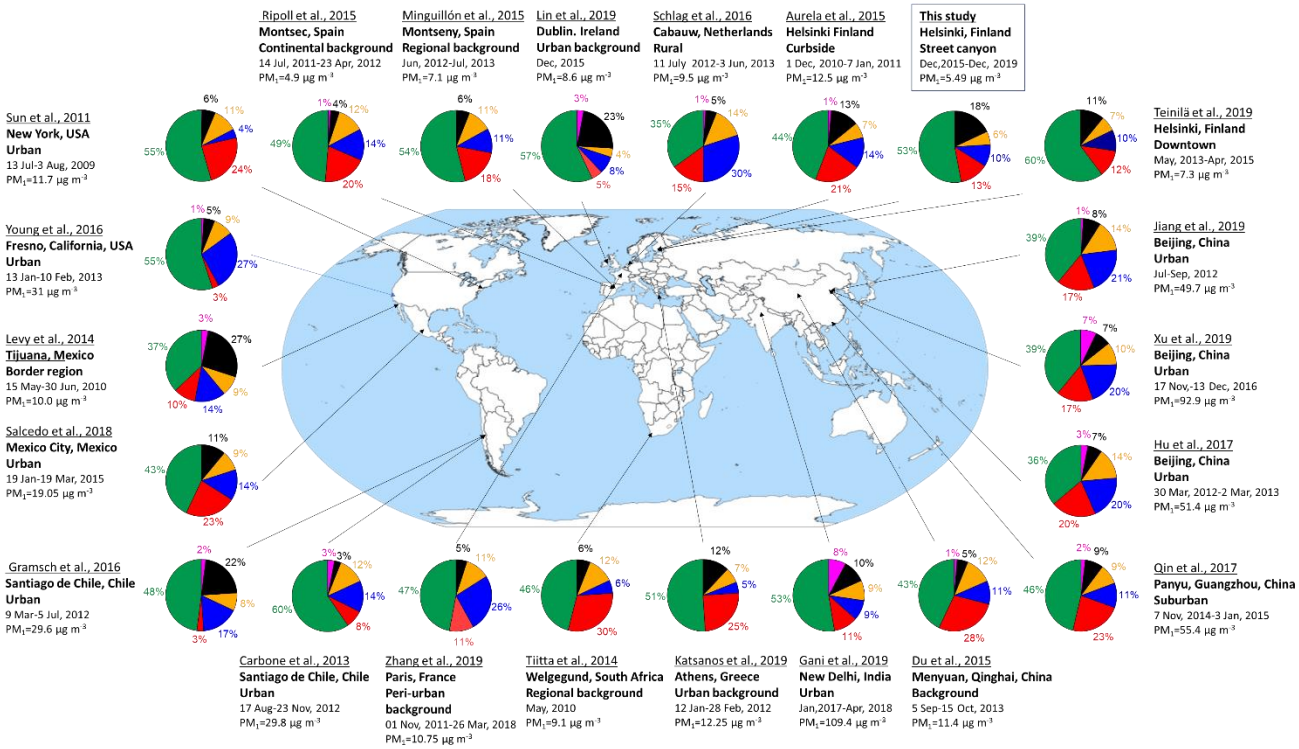

Figure S6: PM_1 characterization determined by other studies performed over the globe in the last years (Green=organics; red=SO_4; blue=NO_3; yellow=NH_4; black=eBC). The world map image was taken from Wikimedia commons (https://commons.wikimedia.org/wiki/File:World_map_blank_with_blue_sea.svg).

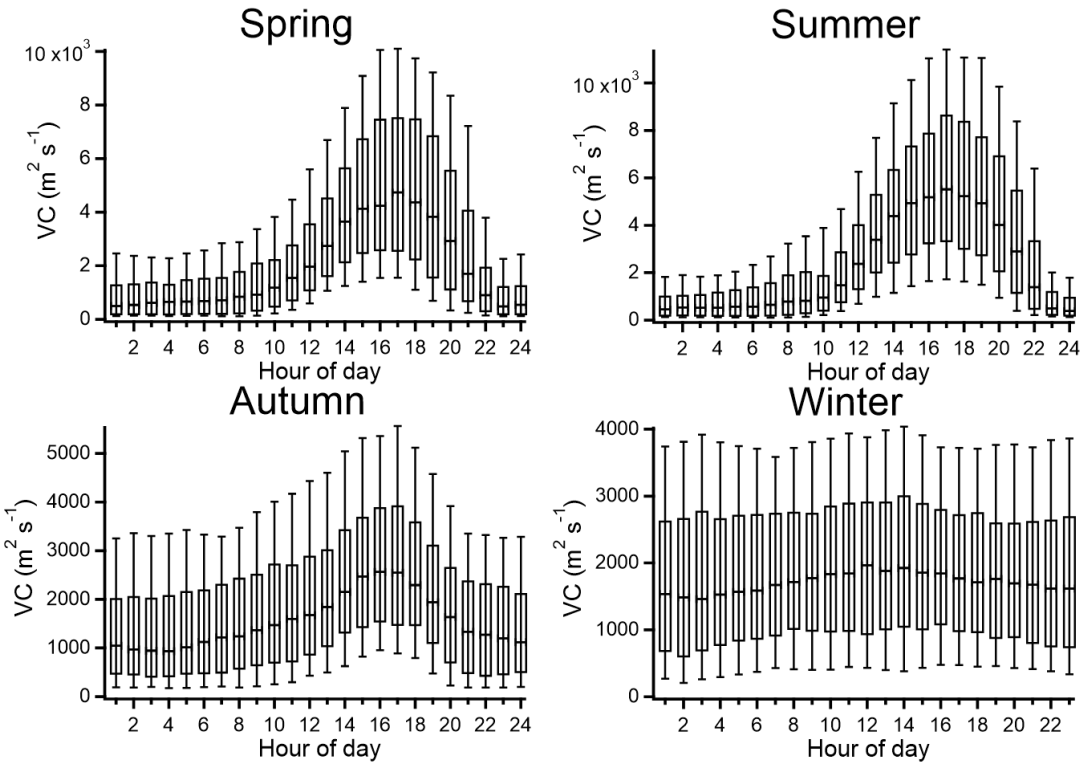

Figure S7: Hourly variation of VC during the four seasons of the year. Note the different scales of y-axis. In each box, the mid-line shows the median value for each x-value component, whisker bottom and top correspond to the 10th and 90th percentiles, and box top and bottom correspond to 75th and 25th percentiles respectively.

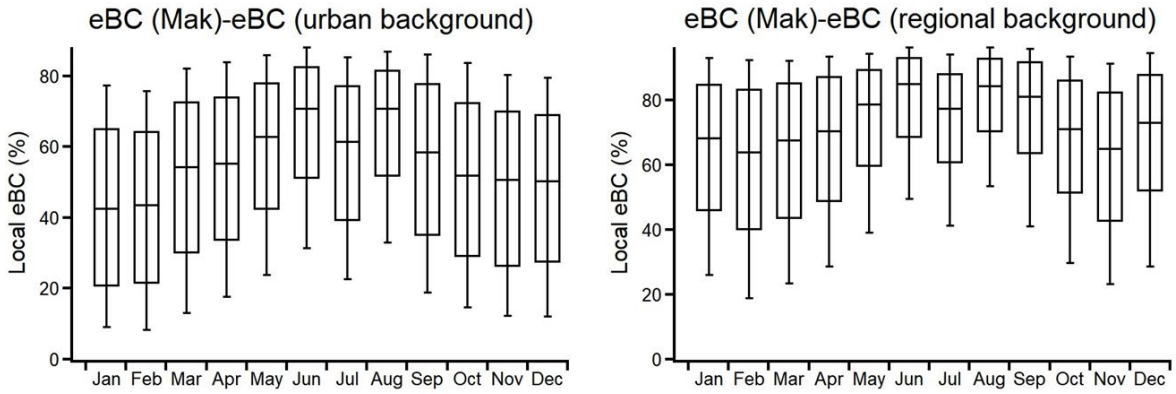

Figure S8: Monthly variation of local eBC at the sampling site. Local contribution of eBC was calculated by subtracting eBC measured at an urban background site (Kallio, left) and at a regional background site (Luukki, right) (Luoma et al., 2020) from the eBC measured at the street canyon site, and the remaining eBC was divided by the street canyon eBC concentration. In each box, the mid-line shows the median value for each x-value component, whisker bottom and top correspond to the 10th and 90th percentiles, and box top and bottom correspond to 75th and 25th percentiles respectively.

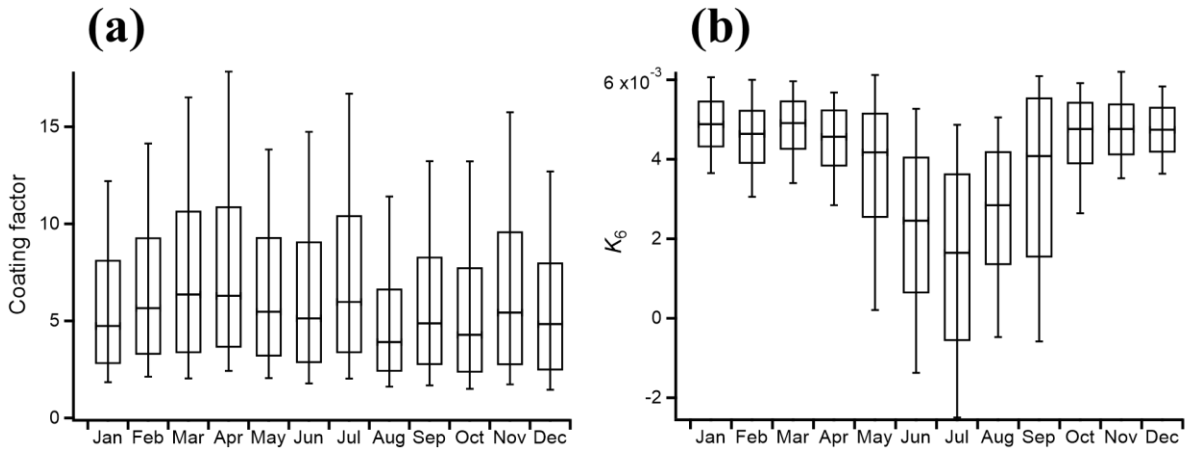

Figure S9: Monthly variation of coating factor (a) and compensation parameter (K_6, (b)). In each box, the mid-line shows the median value for each x-value component, whisker bottom and top correspond to the 10th and 90th percentiles, and box top and bottom correspond to 75th and 25th percentiles respectively.

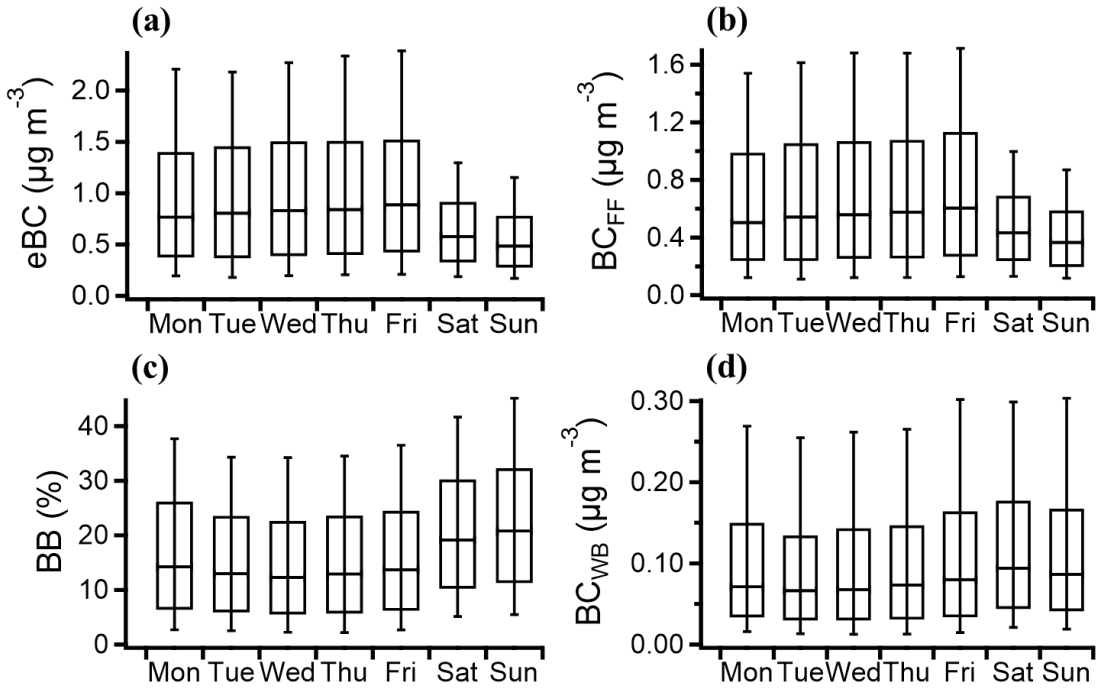

Figure S10: Week variability of eBC (measured by MAAP), BC_{FF}, BB and BC_{WB} (determined by Aethalometer). In each box, the mid-line shows the median value for each x-value component, whisker bottom and top correspond to the 10^{th} and 90^{th} percentiles, and box top and bottom correspond to 75^{th} and 25^{th} percentiles respectively.

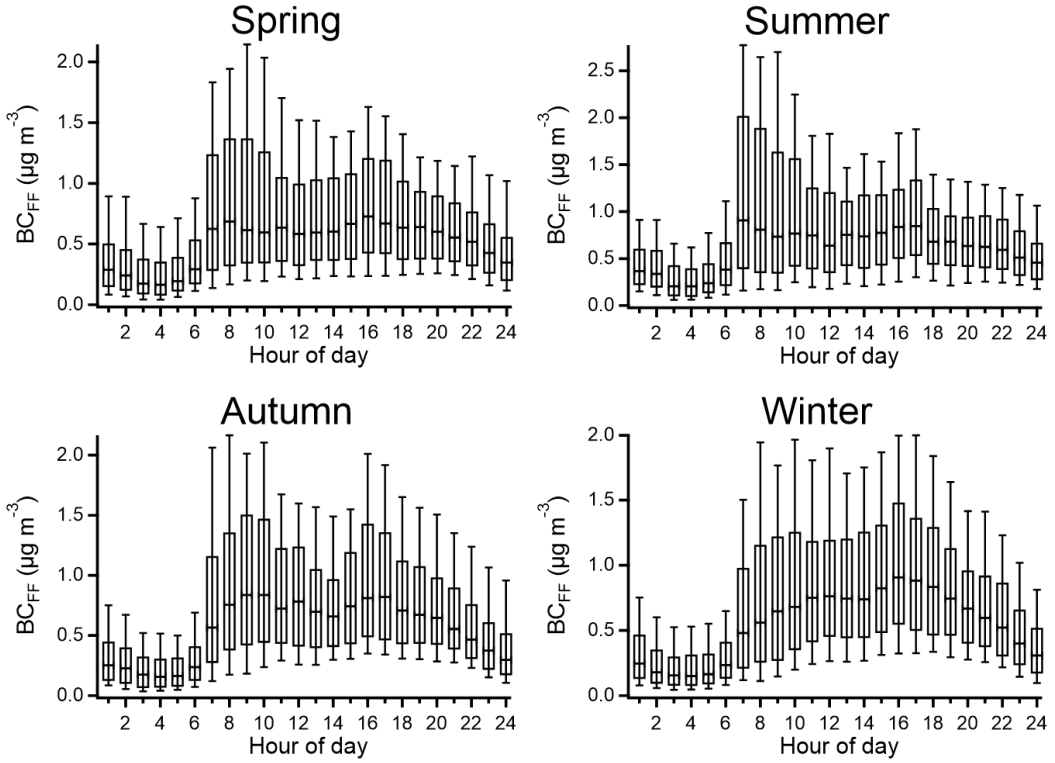

Figure S11: Diurnal variation of BC_{FF} during the different seasons of the year (Spring, Summer, Autumn and Winter). In each box, the mid-line shows the median value for each x-value component, whisker bottom and top correspond to the 10^{th} and 90^{th} percentiles, and box top and bottom correspond to 75^{th} and 25^{th} percentiles respectively.

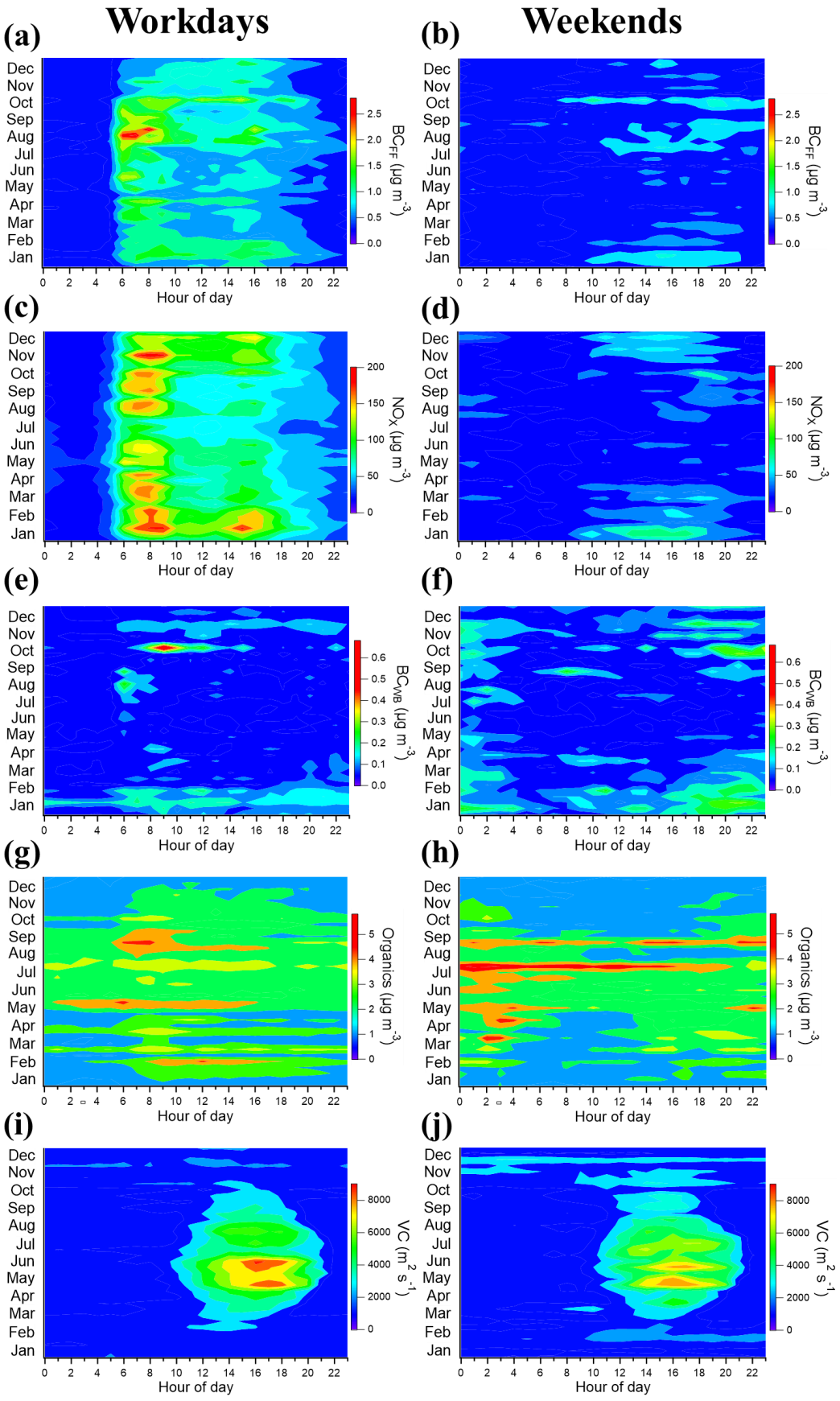

Figure S12: Diurnal and monthly variations of hourly median BC_{FF}, NO_x, BC_{WB}, organics and VC during workdays (left plots) and weekends (right plots).

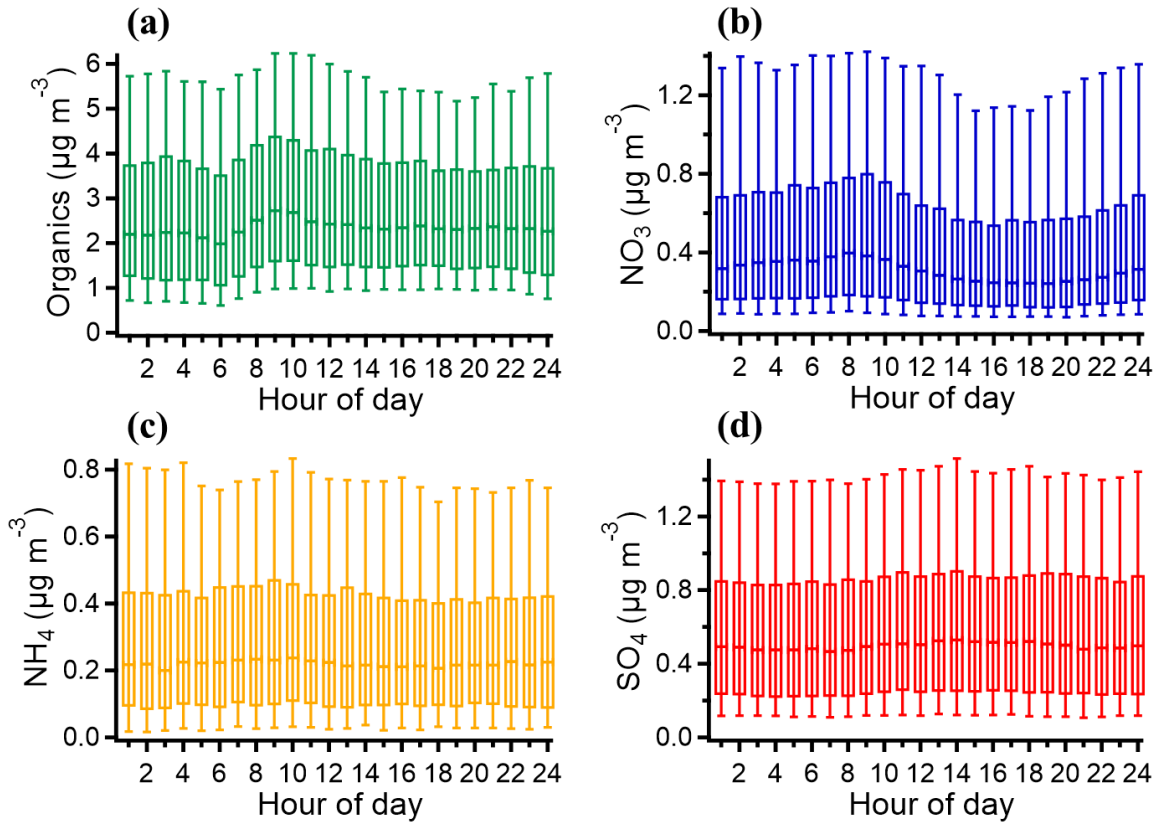

59

60 **Figure S13: Diurnal variation of NR-PM$_1$ constituents (Organics, NO$_3$, NH$_4$ and SO$_4$). In each box, the mid-line shows**
61 **the median value for each x-value component, whisker bottom and top correspond to the 10th and 90th percentiles, and**
62 **box top and bottom correspond to 75th and 25th percentiles respectively.**
63

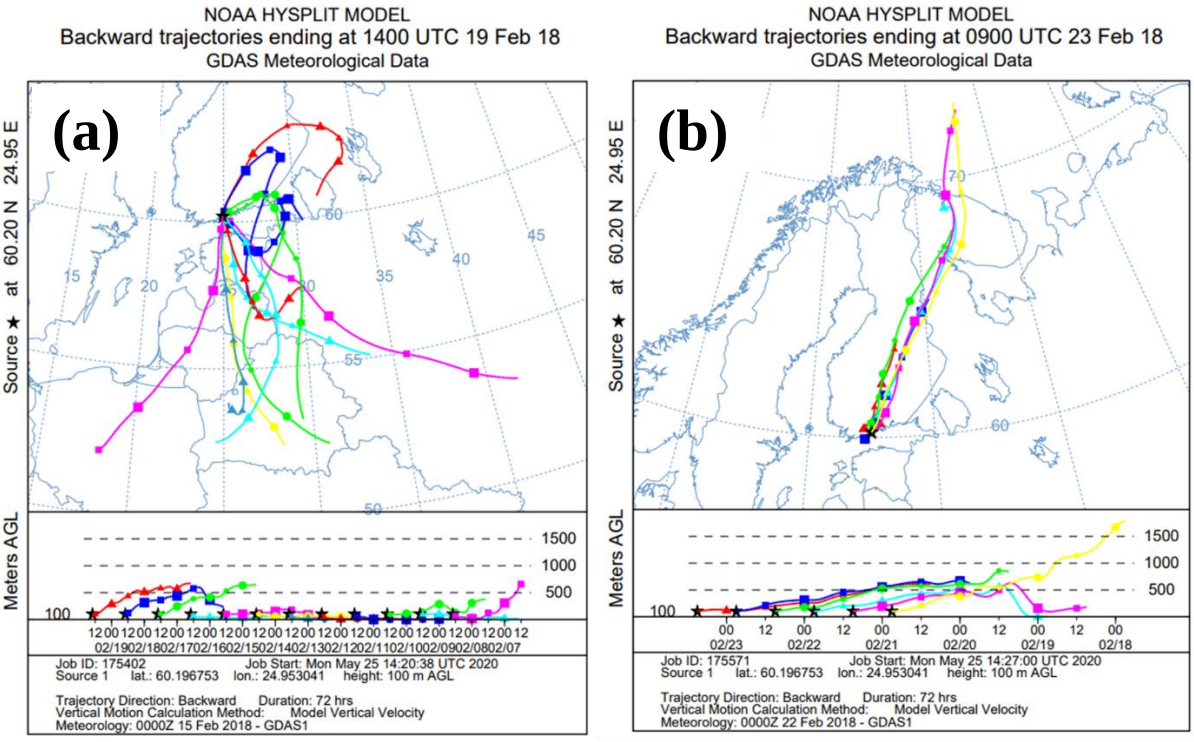

64

65 **Figure S14: Back trajectories observed during the measurement period for the long-range transport event (a) and for**
66 **the local pollution event (b).**

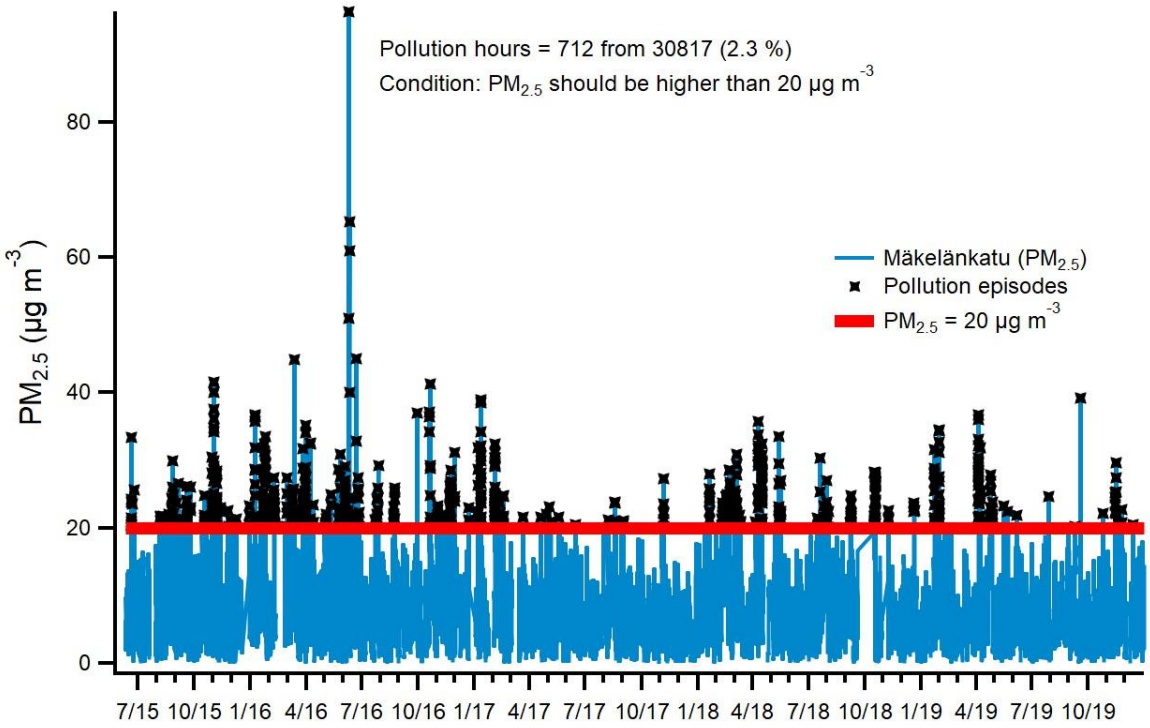

67

68 **Figure S15: Criteria used for evaluating the most intense pollution events occurring in Helsinki during the**
69 **measurement period.**
70

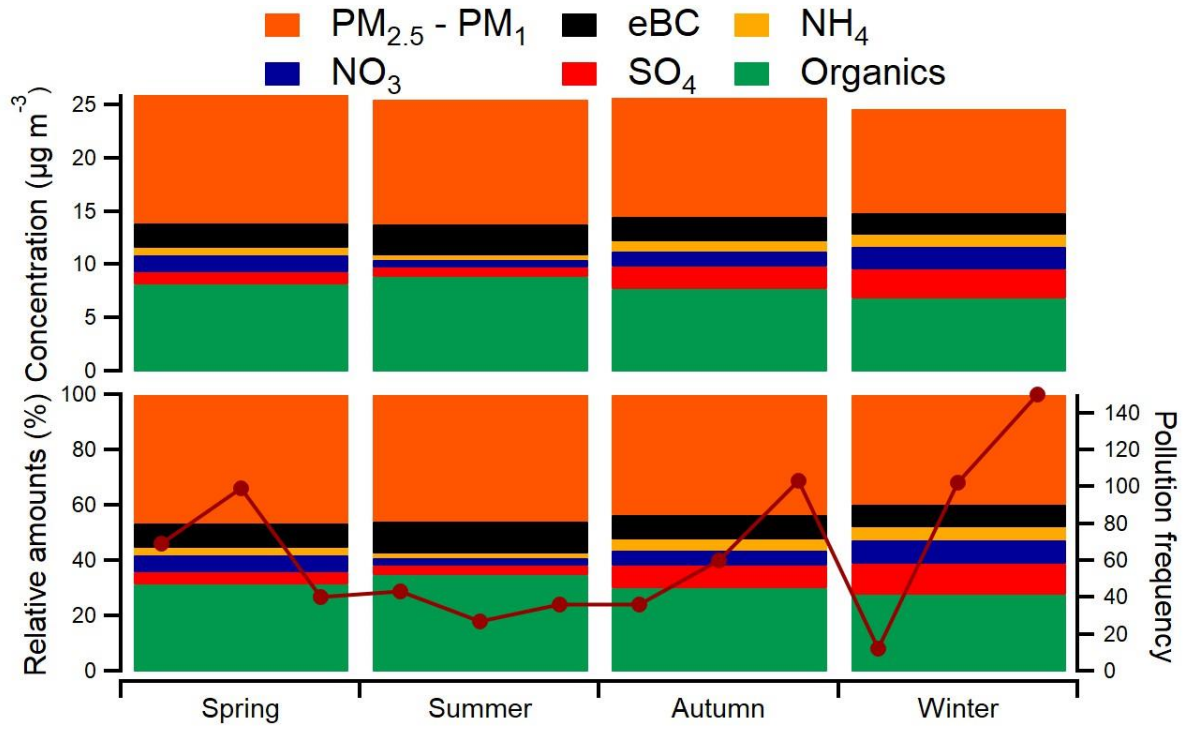

71

72 **Figure S16: Seasonal variation in atmospheric aerosol particle constituent's median concentration and their**
73 **corresponding relative amounts during the pollution episodes. The monthly pollution frequency was also included**
74 **(brown line); Mar–May in spring, Jun–Aug in summer, Sep–Nov in autumn, and Dec–Feb in winter.**

75

S2 Meteorology at the Supersite station during the measurement period in 2015─2019

The meteorological parameters measured during the period of 2015–2019 were evaluated to gain information on the influence of local meteorological conditions on observed aerosol particle concentrations. The minimum temperature was -24.5 °C (January 1st, 2016) and the maximum temperature was +30.8 °C (August 2nd, 2018). The coldest month was January 2016 (-8.6 °C), which was exceptionally cold. On the other hand, the warmest month was July 2018 (21.5 °C) that broke the earlier record of high monthly average temperature in Helsinki. Generally, the coldest month in Helsinki is February with average temperature of -7.0 °C (1981–2010, https://www.ilmatieteenlaitos.fi/helmikuu) and the warmest month is July with average temperature of 17.8 °C (1981–2010, https://www.ilmatieteenlaitos.fi/heinakuu).

The relative humidity (RH) stayed mostly around 75–80 % during wintertime, while the driest periods were observed in May with monthly average RH of 48–54 %. The values are close to what is commonly observed in Helsinki. During the coldest seasons of the year, RH is usually about 90 %, while in spring and summer RH is around 65 % (Pirinen et al., 2012). Wet deposition also influences significantly the measured atmospheric concentrations by washing out the particles during precipitation events. During this study, the rainiest months were between June to September, with maximum monthly precipitation sum observed in June 2016 (150,9 mm). This result is in line with statistics from Helsinki between years 1981 and 2010, showing that the maximums of monthly average rain accumulations are observed in August (80 mm) (https://www.ilmatieteenlaitos.fi/elokuu).

The maximum monthly average wind speeds were observed during winter with values between 5–5.5 m/s, while summertime average wind speeds were between 3.4–4.5 m s^{-1}. Although the winds were stronger in wintertime, the surface layer of atmosphere is usually more stable in wintertime than in summertime and mixing in vertical direction is then more efficient during summer. The prevailing wind direction was south. The sampling site was thus severely affected by pollutants transported from other regions of Europe.

The planetary boundary layer height (PBLH) had a strong seasonal variation, as expected in northern latitudes where seasonality is particularly evident. The mixing height was relatively constant during wintertime, with the median value of about 400 m. This value is consistent with stagnant conditions during this time of the year, favoring the accumulation of PM in a relatively shallow boundary layer. On the other hand, summertime mixing-heights had the lowest yearly values during night and early mornings (23h–10h) but increased rapidly up to above 2000 m during afternoon promoting dilution of atmospheric pollutants. The role of atmospheric dilution in pollutant concentrations was evaluated by determining the ventilation coefficient (VC=wind speed x PBLH), that has been often used in other studies as a parameter to characterize pollutants dilution (e.g. Gani et al., 2019; Sujatha et al., 2016). The VC dilution rate was much lower during the coldest periods of the year (Fig. S7), contributing to increased amounts of PM. The highest VC during spring and summer coincides with an increase in temperature and solar radiation that enhances convection and PBL growth.

References

Aurela, M., Saarikoski, S., Niemi, J. V., Canonaco, F., Prevot, A. S. H., Frey, A., Carbone, S., Kousa, A. and Hillamo, R.: Chemical and Source Characterization of Submicron Particles at Residential and Traffic Sites in the Helsinki Metropolitan Area, Finland, Aerosol Air Qual. Res., 15(4), 1213–1226, doi:10.4209/aaqr.2014.11.0279, 2015.

Carbone, S., Saarikoski, S., Frey, A., Reyes, F., Reyes, P., Castillo, M., Gramsch, E., Oyola, P., Jayne, J., Worsnop, D. R. and others: Chemical characterization of submicron aerosol particles in Santiago de Chile, Aerosol Air Qual. Res, 13(2), 462–473, doi:10.4209/aaqr.2012.10.0261, 2013.

Du, W., Sun, Y. L., Xu, Y. S., Jiang, Q., Wang, Q. Q., Yang, W., Wang, F., Bai, Z. P., Zhao, X. D. and Yang, Y. C.: Chemical characterization of submicron aerosol and particle growth events at a national background site (3295 m a.s.l.) on the Tibetan Plateau, Atmos. Chem. Phys., 15(18), 10811–10824, doi:10.5194/acp-15-10811-2015, 2015.

Gani, S., Bhandari, S., Seraj, S., Wang, D. S., Patel, K., Soni, P., Arub, Z., Habib, G., Hildebrandt Ruiz, L. and Apte, J. S.: Submicron aerosol composition in the world's most polluted megacity: the Delhi Aerosol Supersite study, Atmos. Chem. Phys., 19(10), 6843–6859, doi:10.5194/acp-19-6843-2019, 2019.

Gramsch, E., Reyes, F., Vásquez, Y., Oyola, P. and Rubio, M. A.: Prevalence of Freshly Generated Particles during Pollution Episodes in Santiago de Chile, Aerosol Air Qual. Res., 16(9), 2172–2185, doi:10.4209/aaqr.2015.12.0691, 2016.

Hu, W., Hu, M., Hu, W.-W., Zheng, J., Chen, C., Wu, Y. and Guo, S.: Seasonal variations in high time-resolved chemical compositions, sources, and evolution of atmospheric submicron aerosols in the megacity Beijing, Atmos. Chem. Phys., 17(16), 9979–10000, doi:10.5194/acp-17-9979-2017, 2017.

Jiang, Q., Wang, F. and Sun, Y.: Analysis of Chemical Composition, Source and Processing Characteristics of Submicron Aerosol during the Summer in Beijing, China, Aerosol Air Qual. Res., 19(6), 1450–1462, doi:10.4209/aaqr.2018.12.0480, 2019.

Katsanos, D., Bougiatioti, A., Liakakou, E., Kaskaoutis, D. G., Stavroulas, I., Paraskevopoulou, D., Lianou, M., Psiloglou, B. E., Gerasopoulos, E., Pilinis, C. and Mihalopoulos, N.: Optical Properties of Near-Surface Urban Aerosols and their Chemical Tracing in a Mediterranean City (Athens), Aerosol Air Qual. Res., 19(1), 49–70, doi:10.4209/aaqr.2017.11.0544, 2019.

Levy, M. E., Zhang, R., Zheng, J., Tan, H., Wang, Y., Molina, L. T., Takahama, S., Russell, L. M. and Li, G.: Measurements of submicron aerosols at the California–Mexico border during the Cal–Mex 2010 field campaign, Atmos. Environ., 88, 308–319, doi:10.1016/j.atmosenv.2013.08.062, 2014.

Lin, C., Ceburnis, D., Huang, R.-J., Xu, W., Spohn, T., Martin, D., Buckley, P., Wenger, J., Hellebust, S., Rinaldi, M., Facchini, M. C., O'Dowd, C. and Ovadnevaite, J.: Wintertime aerosol dominated by solid-fuel-burning emissions across Ireland: insight into the spatial and chemical variation in submicron aerosol, Atmos. Chem. Phys., 19(22), 14091–14106, doi: 10.5194/acp-19-14091-2019, 2019.

Minguillón, M. C., Ripoll, A., Pérez, N., Prévôt, A. S. H., Canonaco, F., Querol, X. and Alastuey, A.: Chemical characterization of submicron regional background aerosols in the western Mediterranean using an Aerosol Chemical Speciation Monitor, Atmos. Chem. Phys., 15(11), 6379–6391, doi:10.5194/acp-15-6379-2015, 2015.

Pirinen, P., Simola, H., Aalto, J., Kaukoranta, J. P., Karlsson, P. and Ruuhela, R.: Statistics on the Finnish climate 1981-2010, Finnish Meteorological Institute, 2012.

Qin, Y. M., Tan, H. B., Li, Y. J., Schurman, M. I., Li, F., Canonaco, F., Prévôt, A. S. H. and Chan, C. K.: Impacts of traffic emissions on atmospheric particulate nitrate and organics at a downwind site on the periphery of Guangzhou, China, Atmos. Chem. Phys., 17(17), 10245–10258, doi:10.5194/acp-17-10245-2017, 2017.

Ripoll, A., Minguillón, M. C., Pey, J., Jimenez, J. L., Day, D. A., Sosedova, Y., Canonaco, F., Prévôt, A. S. H., Querol, X. and Alastuey, A.: Long-term real-time chemical characterization of submicron aerosols at Montsec (southern Pyrenees, 1570 m a.s.l.), Atmos. Chem. Phys., 15(6), 2935–2951, doi:10.5194/acp-15-2935-2015, 2015.

Salcedo, D., Alvarez-Ospina, H., Peralta, O. and Castro, T.: PM1 Chemical Characterization during the ACU15 Campaign, South of Mexico City, Atmosphere, 9(6), 232, doi:10.3390/atmos9060232, 2018.

Schlag, P., Kiendler-Scharr, A., Blom, M. J., Canonaco, F., Henzing, J. S., Moerman, M., Prévôt, A. S. H. and Holzinger, R.: Aerosol source apportionment from 1-year measurements at the CESAR towerin Cabauw, the Netherlands, Atmos. Chem. Phys., 16(14), 8831–8847, doi:10.5194/acp-16-8831-2016, 2016.

Sujatha, P., Mahalakshmi, D. V., Ramiz, A., Rao, P. V. N. and Naidu, C. V.: Ventilation coefficient and boundary layer height impact on urban air quality, edited by Z. Wang, Cogent Environ. Sci., 2(1), doi:10.1080/23311843.2015.1125284, 2016.

Sun, Y.-L., Zhang, Q., Schwab, J. J., Demerjian, K. L., Chen, W.-N., Bae, M.-S., Hung, H.-M., Hogrefe, O., Frank, B., Rattigan, O. V. and Lin, Y.-C.: Characterization of the sources and processes of organic and inorganic aerosols in New York city with a high-resolution time-of-flight aerosol mass apectrometer, Atmos. Chem. Phys., 11(4), 1581–1602, doi:10.5194/acp-11-1581-2011, 2011.

Teinilä, K., Aurela, M., Niemi, J. V., Kousa, A., Petäjä, T., Järvi, L., Hillamo, R., Kangas, L., Saarikoski, S. and Timonen, H.: Concentration variation of gaseous and particulate pollutants in the Helsinki city centre — observations from a two-year campaign from 2013–2015, Boreal Env. Res., 24, 22, 2019.

Tiitta, P., Vakkari, V., Croteau, P., Beukes, J. P., van Zyl, P. G., Josipovic, M., Venter, A. D., Jaars, K., Pienaar, J. J., Ng, N. L., Canagaratna, M. R., Jayne, J. T., Kerminen, V.-M., Kokkola, H., Kulmala, M., Laaksonen, A., Worsnop, D. R. and Laakso, L.: Chemical composition, main sources and temporal variability of PM $_1$ aerosols in southern African grassland, Atmos. Chem. Phys., 14(4), 1909–1927, doi:10.5194/acp-14-1909-2014, 2014.

Xu, W., Sun, Y., Wang, Q., Zhao, J., Wang, J., Ge, X., Xie, C., Zhou, W., Du, W., Li, J., Fu, P., Wang, Z., Worsnop, D. R. and Coe, H.: Changes in Aerosol Chemistry From 2014 to 2016 in Winter in Beijing: Insights From High-Resolution Aerosol Mass Spectrometry, J. Geophys. Res. Atmos., 124(2), 1132–1147, doi:10.1029/2018JD029245, 2019.

Young, D. E., Kim, H., Parworth, C., Zhou, S., Zhang, X., Cappa, C. D., Seco, R., Kim, S. and Zhang, Q.: Influences of emission sources and meteorology on aerosol chemistry in a polluted urban environment: results from DISCOVER-AQ California, Atmos. Chem. Phys., 16(8), 5427–5451, doi:10.5194/acp-16-5427-2016, 2016.

Zhang, Y., Favez, O., Petit, J.-E., Canonaco, F., Truong, F., Bonnaire, N., Crenn, V., Amodeo, T., Prévôt, A. S. H., Sciare, J., Gros, V. and Albinet, A.: Six-year source apportionment of submicron organic aerosols from near-continuous highly time-resolved measurements at SIRTA (Paris area, France), Atmos. Chem. Phys., 19(23), 14755–14776, doi: 10.5194/acp-19-14755-2019, 2019.